Two-level systems in superconducting quantum devices due to trapped quasiparticles

(article starts on next page)

CONDENSED MATTER PHYSICS

Two-level systems in superconducting quantum devices due to trapped quasiparticles

S. E. de Graaf[1]*, L. Faoro[2,3], L. B. Ioffe[3,4], S. Mahashabde[5], J. J. Burnett[1], T. Lindström[1], S. E. Kubatkin[5], A. V. Danilov[5], A. Ya. Tzalenchuk[1,6]

A major issue for the implementation of large-scale superconducting quantum circuits is the interaction with interfacial two-level system (TLS) defects that lead to qubit parameter fluctuations and relaxation. Another major challenge comes from nonequilibrium quasiparticles (QPs) that result in qubit relaxation and dephasing. Here, we reveal a previously unexplored decoherence mechanism in the form of a new type of TLS originating from trapped QPs, which can induce qubit relaxation. Using spectral, temporal, thermal, and magnetic field mapping of TLS-induced fluctuations in frequency tunable resonators, we identify a highly coherent subset of the general TLS population with a low reconfiguration temperature ∼300 mK and a nonuniform density of states. These properties can be understood if the TLS are formed by QPs trapped in shallow subgap states formed by spatial fluctutations of the superconducting order parameter. This implies that even very rare QP bursts will affect coherence over exponentially long time scales.

INTRODUCTION

It is becoming increasingly evident that the most coherence-limiting two-level systems (TLS) reside outside the qubit junctions on the surface of metals and dielectrics surrounding them (*1–5*) and their slowly fluctuating dynamics poses a serious challenge for quantum computation (*1, 5–8*). A wide range of techniques has been developed to study such TLS by developing qubits and resonators into probes of a wide range of material properties (*2, 5, 9–15*). At the same time, charged surface TLS and paramagnetic impurities also result in a stochastic and locally varying backdrop for quasiparticles (QPs) in the superconductor itself. It is thus important to consider the implications this backdrop has on the ever-present excess number of nonequilibrium QPs (*16–18*), which must be eliminated to increase qubit dephasing times. It is also likely that such trapped QPs contribute to the number of excess QPs that are responsible for the recently observed (*16*) nonequilibrium relaxation in transmons. Nonequilibrium QPs can be generated by electromagnetic (*19*) and ionizing (*20, 21*) radiation and from rare high-energy cosmic particles impinging the sample, the latter inducing correlated errors in all qubits of a surface code architecture (*22, 23*). When such QPs relax in energy and fall into traps before they can recombine, an exponentially long period of excess decoherence will follow (*24*).

Here, we reveal the implications that a spatially fluctuating superconducting order parameter, Δ, has on trapping of these QPs. Scanning tunneling spectroscopy studies typically find spatial variations in Δ of the order of $\delta\Delta = 10$ to 20% in moderately disordered superconductors (*25–27*). $\delta\Delta$ gets smaller in very clean superconductors; however, even in exceptionally clean films with negligible intrinsic magnetic disorder, an ever-present surface spin density of the order of $\sim 5 \times 10^{17}\,\mathrm{m}^{-2}$ (*2, 28, 29*) results in both flux noise (*2, 29–33*) and spatially nonuniform gap suppression (*28*). In thin films, the gap is also nonuniformly suppressed by the Altshuler-Aronov effect due to impurity scattering (*25, 34*) as well as thickness variations (*35*), particularly relevant for Al (*36*), where recent experiments also reveal subgap states and charge localization across multiple grains (*37*). The clean, low-resistance NbN films that we chose to study in this work are characterized by a low carrier density (*38*). In such materials, it is very likely that the density of states (DOS) varies significantly, resulting in gap variations.

Crucially, we find that the optimal fluctuation able to trap a QP only has a few bound states. As a result, a trapped QP behaves similar to "textbook" TLS, as shown in Fig. 1. We hereafter refer to this type of QP TLS as "qTLS," which coexist with a large number of conventional glassy TLS. The spatial extent of the gap fluctuation sets the frequency of the qTLS, which means that the DOS of these objects is very nonuniform (in contrast to conventional TLS in glasses). We predict a maximum in the qTLS DOS around 6 to 10 GHz, the frequency range of most qubits (transmons). Relatively shallow traps also imply that even a modest temperature can reshuffle the QPs. We expect the underlying qualitative physics of charge defects formed by trapped QPs to be applicable to most materials, including superconductors in the dirty limit, such as Al used for qubits, but the relevant frequency ranges may differ somewhat owing to different material parameters.

This model is supported by a series of experimental observations from detailed mapping of parameter fluctuations in high-*Q* frequency tunable superconducting NbN resonators (*39*). Such resonators allow us to map individual TLS in energy and trace them in a broad range of external parameters, such as magnetic or electric field (*5*). Through analysis of a large number of individual TLS, we find that (i) most qTLS are highly coherent, some with detected linewidths down to ≲70 kHz, the resonator linewidth; (ii) the qTLS landscape irreversibly reshuffles at very modest temperatures of ∼300 mK; (iii) the qTLS DOS appears strongly suppressed at lower frequencies; and (iv) tracking of qTLS in magnetic field reveals a qTLS energy that scale in a way similar to the expected scaling of Δ. In particular, the presence of a low-energy scale, ≲1 K, is inconsistent with conventional TLS theory in which all scales are set by chemical energies (*40*).

[1]National Physical Laboratory, Hampton Road, Teddington TW11 0LW, UK. [2]Sorbonne Université, Laboratoire de Physique Théorique et Hautes Énergies, UMR 7589 CNRS, Tour 13, 5eme Etage, 4 Place Jussieu, F-75252 Paris 05, France. [3]Department of Physics, University of Wisconsin-Madison, Madison, WI 53706, USA. [4]Google Inc., Venice, CA 90291, USA. [5]Department of Microtechnology and Nanoscience, MC2, Chalmers University of Technology, SE-41296 Goteborg, Sweden. [6]Royal Holloway, University of London, Egham TW20 0EX, UK.
*Corresponding author. Email: sdg@npl.co.uk
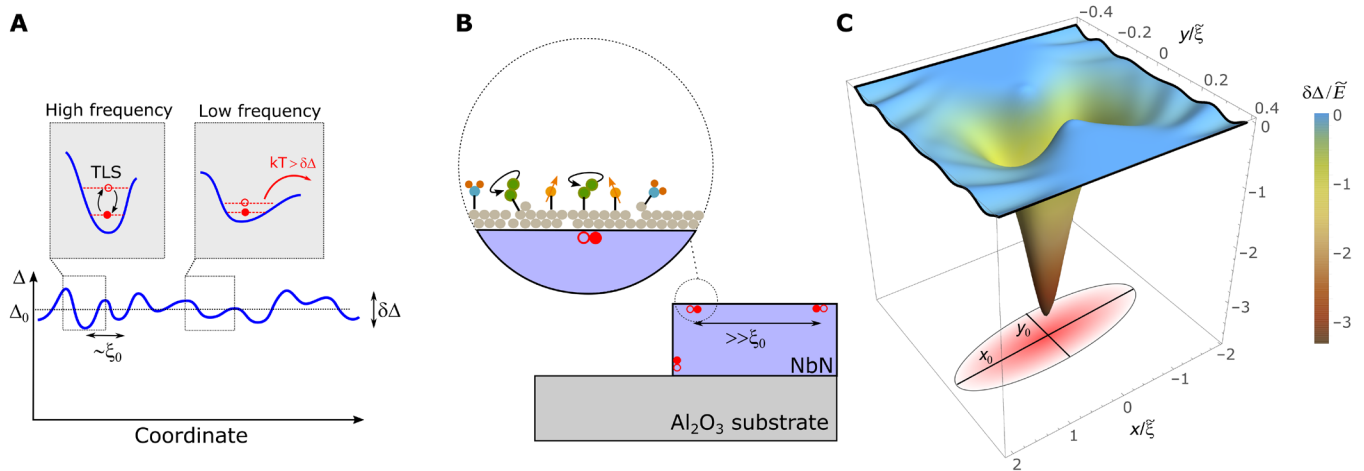
Fig. 1. qTLS formation. (**A**) Illustration of typical fluctuations of the order parameter Δ and the formation of wells with multiple bound states in which QPs can be trapped, effectively forming a TLS (qTLS). The scale of the trap determines the qTLS frequency and escape rate. (**B**) qTLS are separated by large distances compared to length scales at which fluctuations in Δ occur, fluctuations that may originate from impurity scattering or surface spins. The qTLS are separated by a distance from the superconductor oxide surface where conventional TLS defects, adsorbates, etc. reside and form the usual bath of TLS. (**C**) Numerically evaluated typical elongated single-well fluctuation of the order parameter capable of hosting multiple bound states for QPs, forming a qTLS. Here, $\widetilde{\xi} = \sqrt{\Delta_0/E}\,\xi_0$, the scaling assumes $(k_F\xi_0)^{-1} = 0.014$, $\Delta_0/E = 40$, appropriate for our NbN samples.

The low-energy scale is instead natural for TLS formed by QPs trapped in regions of locally depressed gap. We start by outlining the main features of the model that explains these observations.

RESULTS

To understand the emergence of qTLS from a fluctuating $\Delta = \Delta_0 + \delta\Delta(\mathbf{r})$, we consider a general model that assumes Gaussian fluctuations of the gap, $\langle \delta\Delta(\mathbf{r})\delta\Delta(\mathbf{r}') \rangle = g\delta(\mathbf{r} - \mathbf{r}')$, where $g \simeq \delta\Delta\Delta_0\xi_0^2$ is the strength of fluctuations and ξ_0 is the Bardeen-Cooper-Schrieffer coherence length. The exact origin of these fluctuations is not relevant for the conclusions. The density of subgap states is determined by rare fluctuations of the gap that reduce the QP energy sufficiently below the gap edge in a uniform material. The key point is that such fluctuations can create traps with a shape and depth that allow them to effectively trap QPs. As the QPs near the gap edge move with momenta close to the Fermi momentum p_F, it follows that trapped QPs will have similar momenta, which can point in an arbitrary direction. This freedom results in the optimal trap being very anisotropic, with a shape elongated along the direction of p_F. In Fig. 1C, we show the typical shape of such a trap obtained through numerical simulations. In general, the probability to find a fluctuation of depth E scales exponentially with the area A of the fluctuation, $P \sim \exp(-E^2A)$. The most likely traps thus have a small area; however, a too small dimension along the direction of p_F will prohibit the formation of a bound state due to the large kinetic energy of the QP. Therefore, optimal traps do not favor isotropic fluctuations. The wave function of the QP oscillates quickly along the direction of p_F. The ground and excited states in the trap differ in the number of oscillations: Since the total number of oscillations is large, it is not surprising that each trap typically contains more than one bound state; however, the number of bound states is expected to remain small for most traps, and the qTLS considered here typically only has two bound states inside the trap.

Because of the presence of excited bound states, a QP in such a trap forms an effective TLS with typical energy splitting

$\hbar\omega_{qTLS} = \zeta|\widetilde{E}|$, where $\widetilde{E}$ is the energy of the trapped QP as measured from the gap edge and $\zeta \approx 0.7$ is found from theory (see the Supplementary Materials). One consequence of these traps is that, in contrast to conventional TLS, the DOS of qTLS is not constant. A large ω_{qTLS} implies very deep traps that are exponentially rare. We find the density

$$\rho_{qTLS}(\omega) \simeq \nu(\widetilde{E}) = \frac{1}{\xi_0^2\Delta_0}\exp\left[-\frac{\eta}{g}\frac{\xi_0^2\Delta_0^2}{\sqrt{k_F\xi_0}}\left(\frac{\hbar\omega}{\zeta\Delta_0}\right)^{5/4}\right] \quad (1)$$

where $\eta \approx 10$. Likewise, small ω_{qTLS} are suppressed, since QPs in shallow traps annihilate each other efficiently, leading to

$$\rho_{qTLS}(\omega) \leq \nu_0(\widetilde{E}) = \frac{\sqrt{2\,k_F\xi_0}}{\xi_0^2\Delta_0\,[\ln(\tau_{exp}\Delta_0/\hbar)]^2}\left(\frac{\hbar\omega}{\zeta\Delta_0}\right)^{3/4} \quad (2)$$

Here, τ_{exp} is a time scale that determines the steady-state density of qTLS. In the absence of a source, the QP density will vanish logarithmically slow owing to the reduced likelihood of recombination (*24*). In reality, there will be a steady resupply of QPs at the gap edge, as determined by the intensity of the source (*24*). For long measurement times ($\gtrsim$s), this provides a cutoff for the logarithm and results in an equilibrium density of qTLS. For any experimentally relevant scenario, the factor $[\ln(\tau_{exp}\Delta_0/\hbar)]^2$ is on the order of ~1000 (see the Supplementary Materials for details).

In this picture, the TLS is formed in a single well, in contrast to the more conventional double-well picture. Because of the spatial asymmetry, the transition between the lowest and first excited state in each trap is expected to have a significant electric dipole moment, resulting in a strong interaction with quantum devices. Although the size of the gap fluctuation is very large (~ ξ_0^3), the dipole moment of the qTLS is expected to be significantly smaller, as it is directed predominantly along the surface of the superconductor, while electric fields are orthogonal to the surface. Taking into account the screening

of electric fields at atomic length scales, it is natural to expect that the characteristic dipole moment is commensurate with atomic scales.

In moderately clean NbN films, $\delta\Delta$ constitute up to 10% of the total gap 2Δ (25–27), corresponding to $\delta\Delta \approx 2.5$ K. At $T = 10$ mK, tunneling out of such a local minima is exponentially suppressed; however, at temperatures approaching fractions of $\delta\Delta$, there is a finite probability that the QP escapes and either finds another minima or recombines, resulting in a typical escape temperature of the order of 200 to 300 mK, each event resulting in a different TLS landscape.

The unusual shape of the traps and the presence of multiple bound states in each trap distinguish clean superconductors from the dirty limit (41–43). In the latter, a QP is scattered many times by defects while moving in a particular direction inside the trap, making the formation of elongated traps impossible. The physics of qTLS traps is similar to the well-studied phenomena of the appearance of states with negative energy in disordered conductors (44, 45) with two important differences: Electrons at the bottom of the band in a disordered conductor have much smaller momenta, and the wave functions do not have zeros.

We now turn to experiments where our observations can be explained by this model. To be able to study individual TLS and spectral and temporal fluctuations of superconducting resonator parameters, we use kinetic inductance–tunable superconducting resonators with center frequencies f_0 in the range 3 to 7 GHz, described in detail in (39). The resonators are cooled down to a base temperature of 10 mK in a well-filtered dilution refrigerator. A small dc current (<1 mA) is applied to change the kinetic inductance and tune f_0. We measure the transmitted microwave signal, S_{21}, using a vector network analyzer and extract the resonator frequency and quality factors Q. In some of the experiments, we also use a gate electrode mounted in the lid of the sample enclosure (see Fig. 2A), such that we can change the TLS energy through the applied gate voltage V_g: $E_{TLS} = \sqrt{\epsilon_0^2 + \gamma^2 V_g^2}$ (4, 5).

Here, ϵ_0 is the TLS minimum energy and γ the TLS voltage coupling strength.

In Fig. 2B, we show the relative variation of the internal quality factor $\delta Q_i = (Q_i - \langle Q_i \rangle)/\langle Q_i \rangle$, as we tune the resonator frequency. The measurement is continuously repeated over several days to produce a spectral and temporal map of the variations in loss. This reveals large drops in δQ_i: At detunings of 3.5 and 14 MHz (from 6.995 GHz), TLS dips (indicated by horizontal arrows) remain in the same place, whereas, at other frequencies, both switching-like behavior and drift can be observed. We then raise the temperature of the cryostat to 300 mK, repeat the same measurement (Fig. 2C), and return to 10 mK (Fig. 2D). We observe that a strong TLS remains stable over more than 60 hours in each individual measurement, but thermal cycling to a mere 300 mK makes another TLS appear at a different frequency. This is quite remarkable, as the temperature is increased to a value smaller than the energy level splitting of the TLS itself (7 GHz $\approx$ 350 mK) and certainly not expected from conventional TLS glass physics in which all scales are set by chemical energies (40). Separate high-power measurements show that these dips are saturable and not caused by, e.g., local variations in background transmission. We have repeated the same experiment but visiting multiple temperatures on the way to 300 mK (see the Supplementary Materials for additional data and methodology), which confirms that reconfiguration only happens near 300 mK.

Occasionally, we observe very dissipative TLS with linewidths in excess of several megahertz in our measurement window (red arrow in Fig. 2D). Here, we concentrate instead on the much more coherent TLS that we consistently observe, the narrowest with linewidths down to $\sim$70 kHz (see the Supplementary Materials) limited by the readout resonator linewidth. In Fig. 3A, we show the histogram of linewidths of the observed TLS, which peaks at values corresponding to coherence times in excess of several microseconds, much longer than what has been reported for individually resolved TLS in qubits (5, 14). The energy leakage caused by such highly coherent (and strongly coupled) TLS could pose a significant challenge for quantum error correction (46). Naturally, qTLS interact with conventional TLS and slow fluctuators that result in parameter fluctuations.
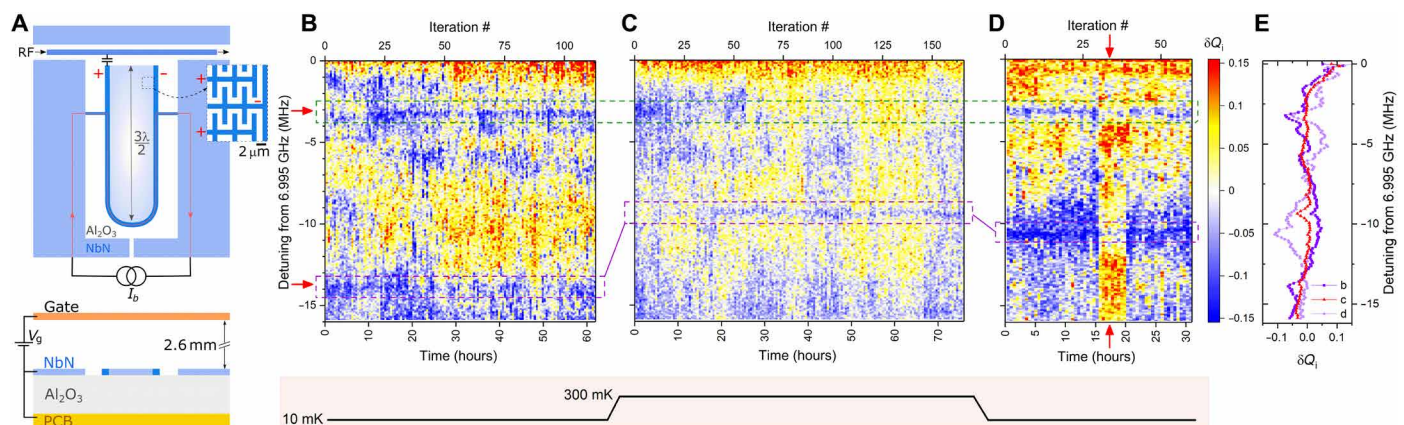
Fig. 2. Spectral and temporal fluctuations of the internal quality factor and spectral reconfiguration of TLS. (**A**) Device sketch showing the plane of the resonator and the current biasing circuit for frequency tuning (top) and device cross section showing the geometry of the electrostatic gate used for TLS tuning. (**B**) Initial measurement taken at 10 mK and average photon number $\langle n \rangle \approx 40$. For each pixel, the resonator line shape is measured and fitted to extract the internal quality factor Q_i. The measurement is repeated as the resonator is tuned in frequency (the typical frequency resolution is ≈ 50 kHz); this measurement versus detuning is then repeated over time. The color scale shows the normalized variation $\delta Q_i = (Q_i - \langle Q_i \rangle)/\langle Q_i \rangle$. Horizontal arrows indicate two static TLS. (**C**) The same measurement performed after (B) with the temperature set to 300 mK. (**D**) The same measurement was repeated again after returning to 10 mK. The red vertical arrow indicates a broad TLS jumping into the measurement window. Dashed boxes indicate two strong TLS. For repeated experiments, see the Supplementary Materials. (**E**) The time-averaged data from (B) to (D).
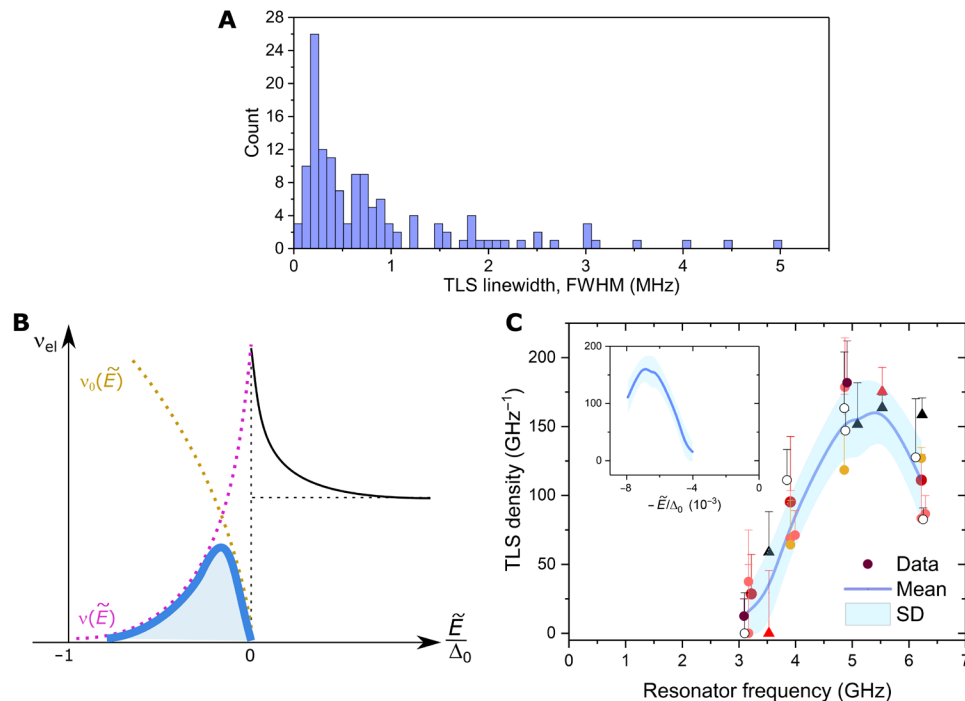
Fig. 3. qTLS properties. (**A**) Histogram of extracted TLS linewidths [full width at half maximum (FWHM)] obtained at 10 mK across a series of cooldowns and different resonators in the frequency range 3 to 7 GHz. (**B**) Theoretically expected scaling of the qTLS DOS (blue solid region) bounded by $\nu(\tilde{E})$ and $\nu_0(\tilde{E})$ (see text for details). Not to scale. (**C**) Number of experimentally detected strongly coupled TLS as a function of frequency. The data points are obtained by counting the number of TLS present in a spectral and temporal map. Data taken on two different samples (circles and triangles) in seven separate cooldowns (different colors). Duplicate markers at the same frequency are before/after thermal reconfiguration. Multiple markers from the same resonator have been offset somewhat in frequency for better visibility. Error bars indicate miscounting the number of TLS by one, e.g., if one TLS happens to be present just outside the measurement range. The solid line is the average of observations, bounded by the SD. The inset shows the same data plotted against the corresponding trap depth from Δ_0. All data are obtained at 10 mK and $\langle N \rangle < 100$.

We now turn to the qTLS DOS. Figure 3B shows the expected frequency dependence of the qTLS DOS, given by the bounds of Eqs. 1 and 2. This reproduces the peaked shape in the DOS of strongly coupled qTLS that we observe in resonators with different f_0, shown in Fig. 3C; data were obtained across several cooldowns and devices.

The quantitative agreement is also satisfactory given the uncertainty in the parameters entering the equations. The expected position for the peak in the TLS density matches the experiment for a gap disorder $\delta\Delta$ of a few percent. This is in agreement with scanning tunneling microscopy data (47) for moderately clean NbN with similar values of T_c and Ioffe-Regel disorder parameter $k_F l$.

A similar frequency dependence on the number of observed qTLS at different frequencies was obtained by tuning the TLS energy by an applied electrostatic field (see the Supplementary Materials). In contrast, for conventional noninteracting TLS in amorphous materials, we expect a DOS $P(E) = \text{const}$ (40), while for interacting TLS, we expect a weak pseudogap given by $P(E) = E^\mu$ (48, 49). $\mu \approx 0.2$ is typically found experimentally (3, 9), which would, for $f_0 = 3$ to 6 GHz, only result in a ~10% variation in the TLS DOS. As expected, we find through the temperature-dependent shift of f_0, which samples all TLS, including the more numerous conventional glassy TLS, that the intrinsic loss tangent falls within $F \tan \delta_i = 0.7 \pm 0.1 \times 10^{-5}$, with no observed dependence on f_0 (see the Supplementary Materials).

The data in Fig. 3C have not been scaled to the surface area occupied by each resonator, which would yield an even stronger nonlinear dependence ($A \propto f_0$); however, this is expected to be balanced by the reduced coupling strength affecting the detectability of individual TLS at lower frequency. If we make the assumption that the observed qTLS uniformly occupy the surface of the superconductor, we get, for $f_0 = 4.9$ GHz, an observed density of qTLS of 0.004 GHz^{-1} μm^{-2} or 1 GHz^{-1} per ($\sim 3000\xi_0$)^2. In our devices, the distance between electrodes in the resonator is small (2 μm) (see Fig. 2A), resulting in significant microwave electric fields away from the immediate vicinity of metal edges. The maximum observed TLS coupling strengths of up to 100 to 200 kHz are obtained for electric dipoles of size $p_0 \sim 1$ eÅ across a significant part of the device surface. Near metal edges, we would expect coupling strengths exceeding 1 MHz (see the Supplementary Materials). This we do not observe, implying instead that the qTLS are detected across most of the device surface. The above density is much smaller than the total density of TLS we extract from $F \tan \delta_i$. We find a surface density of $\rho_{\Delta, A} \approx 50$ GHz^{-1} μm^{-2} of weakly coupled TLS, which are mainly responsible for the background loss and noise (see the Supplementary Materials) previously studied in detail (3, 9). These conventional TLS coexist with the qTLS and constitute the much broader background of loss and fluctuations. However, since the qTLS are located at the metal surface, they interact weakly with the conventional glassy TLS bath, which is mainly situated some distance away, e.g., in the oxide on the superconductor and adsorbates on top, resulting in higher qTLS coherence.

Last, to determine whether there is a link between the qTLS and superconductivity, we measure a strongly coupled qTLS in an applied magnetic field B parallel to the superconducting film, shown

in Fig. 4A. As expected, we observe a quadratic suppression of f_0 owing to the kinetic inductance increasing as Δ is suppressed. At the same time, we track the anticrossing of the qTLS and extract the minimum qTLS energy $\epsilon_0(B)$. As shown in Fig. 4B, ϵ_0 is also suppressed in magnetic field at a scale comparable to the weak (few percent) suppression of Δ. We also note that the conventional TLS bath remains unaffected up to moderate fields (50).

DISCUSSION

High-resolution spectral mapping of individual TLS in qubits has only been performed in the range 5 to 6 GHz (1). Below 3 GHz, the qubit performance in other studies was limited by other loss mechanisms or the statistics was insufficient to demonstrate the presence of individual, strongly coupled TLS (31, 51, 52). As far as we are aware, only (53) hints at a lower TLS density in Al qubits below $\simeq 3$ GHz, suggesting that the mechanism responsible for the formation of qTLS could be quite common and motivating the need to explore lower frequencies.

To assess the applicability to other materials, we note that the parameter g is important for the location of the DOS maximum, whereas other parameters of the superconductor mainly affect the prefactor. The density is expected to be within the same order of magnitude for a range of common materials such as Nb, NbTiN, and TiN and peaked at similar frequencies. Even for Al, the effect of different superconductor parameters results in a relatively small difference. However, g, is, to the best of our knowledge, not known for thin Al films, but it is likely to be enhanced because of, e.g., thickness fluctuations (35, 36). This would, remarkably, make the qTLS DOS for NbN and Al quite similar, despite the otherwise rather different material parameters, provided that the same mechanism is valid in the dirty limit. In the dirty limit and at edges of the superconductor, the details of the theory developed here are not directly applicable. However, we expect that the general mechanism could still apply albeit the optimal shape of fluctuations is likely to be different, resulting in different prefactors to the qTLS DOS.

We now turn to the implications that these qTLS states have for a range of superconducting technologies and for the coherence of qubits. A typical sample of ~1 cm^2 size is hit by a high-energy cosmic ray once in every ~10 s, creating a shower of phonons that quickly relax to low frequencies where their relaxation time becomes very long. These phonons produce QPs well above Δ, which, in turn, relax to the gap edge, and most of these excess QPs quickly recombine. However, when the remaining QPs at these energies become very sparse, their relaxation time is exponentially long. Eventually, the QPs that have relaxed to the gap edge fall into the traps discussed here, where they remain for exponentially long time scales at low temperatures. Such localization of QPs prevents their recombination and equilibration (24). At low temperatures, this trapping (and detrapping) rate becomes very slow; hence, we expect only a fraction of possible qTLS traps to be filled at any given time. The excess QP concentration is essentially independent of the burst rate (24), and the qTLS density would remain the same over long time scales and between cooldowns. Furthermore, the total integrated density of detected qTLS (~10^{11} m^{-2}) is remarkably close to the number of excess QPs, ~10^{10} to 10^{11} m^{-2} (commonly expressed normalized to the Cooper pair density as $x_{qp} \sim 10^{-7}$ to 10^{-8}) as found in a number of experiments (16, 54). Trapped QPs close to a qubit can result in its excitation or relaxation, and hence the QP localization results in a long period of qubit performance degradation. As this degradation can affect all qubits on a sample, it becomes a catastrophic event for quantum computation, a conclusion supported by recent studies of QP bursts in granular Al resonators (17) and kinetic inductance detectors (55).

Identifying and eliminating strongly coupled TLS is crucially important for scaling up of superconducting quantum computing. If high-energy QP bursts cannot be fully eliminated, the expected long period of qubit performance degradation implies that the most effective strategy for improving long-term stability is to reduce the fluctuations in Δ. All the mechanisms that lead to gap fluctuations are difficult to control in thin films used for resonators and qubits, but our results suggest that these must be carefully addressed to achieve this goal. Routes toward minimizing gap fluctuations include finding
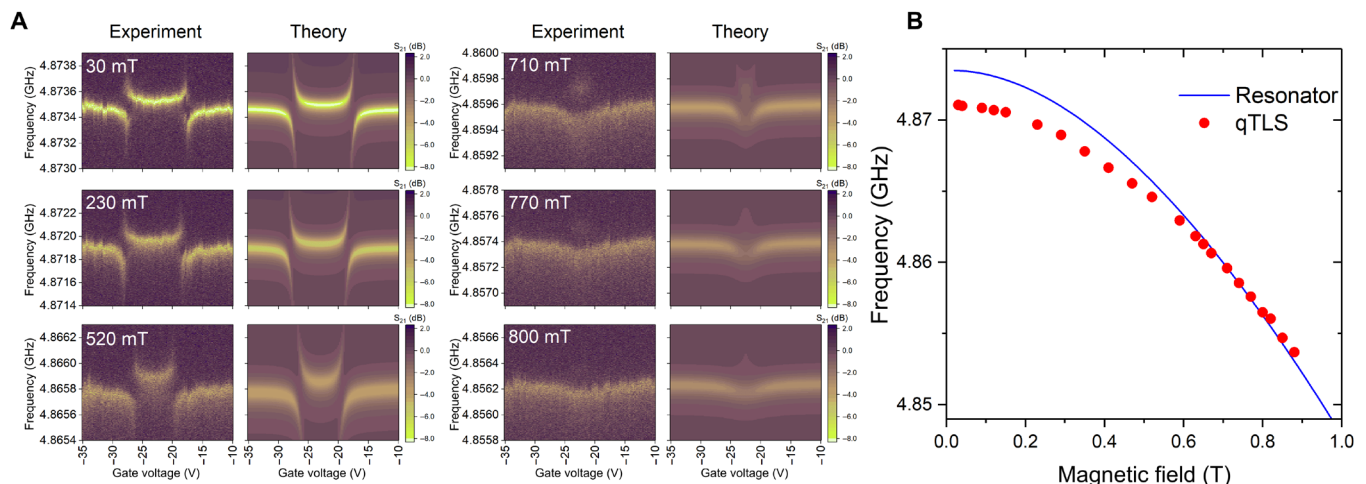
Fig. 4. A single strongly coupled qTLS in magnetic field. (**A**) Transmission spectrum of the resonator strongly coupled to a qTLS at selected magnetic fields, as a function of applied electrostatic gate voltage, showing the coherent coupling of a single qTLS to the resonator. (**B**) The measured resonance frequency as a function of magnetic field (solid blue line) together with the extracted qTLS minimum frequency ϵ_0/h (red markers). Other extracted parameters are as follows: qTLS-resonator coupling strength, $g_0 = 270$ kHz; damping rate, $\gamma_{qTLS} = 200$ kHz and $\gamma = 10$ MHz/V, consistent with $p_0 \approx 1$ eÅ in our sample geometry.

surface treatments that reduce the number of surface paramagnetic impurities and adsorbates (*2*) and developing epitaxial film growth (*56*) and coatings to reduce the number of structural defects in the superconductors and their surface oxides.

In conclusion, we have demonstrated that nonequilibrium QPs present in superconducting quantum devices can be trapped in rare elongated fluctuations in the disorder potential. Such traps have multiple bound states in a single well, which forms an effective TLS. This constitutes a previously unexplored decoherence mechanism originating from nonequilibrium QPs, which poses a significant challenge for quantum computing. This picture is supported by a series of experimental observations of unusual TLS properties: low-energy scales, very high coherence, nonlinear DOS, and an unexpected magnetic field dependence of the TLS energy. We are able to reveal these properties through a combined detailed spectral, temporal, thermal, and magnetic field mapping of a large number of individual qTLS found in planar superconducting NbN resonators.

MATERIALS AND METHODS

Device design and fabrication

The resonator design and fabrication is outlined in detail in (*39*), and the resonators used here are of exactly the same design but of varying length (frequency). The resonator structure is patterned using electron beam lithography from a 140-nm NbN film deposited on a heated 2″ sapphire substrate. The film is etched in a Ar : Cl$_2$ reactive ion plasma, which ensures sharp sidewalls and prevents lateral under-resist etching. Wire bonds for radio frequency and dc connections are facilitated by Au bonding pads, which are deposited in the next step. The resonator (excluding the ground plane) is thinned down to 50 nm in the same Ar : Cl$_2$ reactive ion plasma in the final fabrication step. This yields a sheet kinetic inductance of ~4 pH/□ and places the resonance frequency in the 3- to 8-GHz band. The sheet kinetic inductance of the ground plane is lower than the resonator film, ensuring that the typical frequencies of the ground plane resonances are placed above 8 GHz. Following the last etching step, which produces the final film surface, the residual resist mask is removed in 1165 remover followed by an isopropanol and water rinse. The final step is a soft O$_2$ plasma clean. A second set of samples used to evaluate the TLS density uses a thinner film, 17 nm, with no apparent effect on the qTLS density. The films are characterized by a critical temperature T_c = 14.2 K, a resistivity ρ = 1.6 microhm·m, and an Ioffe-Regel disorder parameter $k_F l \approx 6$ (see the Supplementary Materials for more material-specific data).

Measurement setup and methodology

All measurements were carried out in a cryogen-free dilution refrigerator with a base temperature of 10 mK. The cryostat was equipped with well-filtered coaxial lines, and a high electron mobility transistor amplifier with a noise temperature of ≈3 K was used for readout. The superconducting resonators were measured using a vector network analyzer. Unless otherwise indicated, measurements were carried out at 10 mK with very low excitation powers applied to the resonator, equivalent to ≲100 photons in the resonator, ensuring that TLS are not saturated. The resonator frequency was tuned using a low-noise voltage source in series with a 5-kilohm resistor to produce the required tuning current on the order of 1 mA. The voltage applied to the gate electrode was supplied using a low-noise voltage source connected to a low-pass–filtered thermocoax

line in the cryostat. For further details of the measurement setup and schematics, see the Supplemental Materials. The data presented here and in the Supplementary Materials were collected over more than 10 separate cooldowns and across three different samples.

The magnetic field dependence (Fig. 4) was measured in a separate cooldown, where the sample was mounted in the bore of a 9/1/1 T vector magnet inside the dilution refrigerator. The resonators themselves are highly magnetic field resilient, retaining quality factors in excess of 10^5 above B = 1 T (*39*). To ensure optimal alignment of the magnetic field with the superconducting plane, we applied a small field (5 mT); by rotating the field by a small amount (few degrees) and tracking the resonance frequency as a function of field angle, we find the optimal orientation from the maximum in the resonance frequency. The experiments were carried out at zero current detuning; we instead tune the TLS into resonance using the electrostatic gate in the sample enclosure. The reason for this was purely technical; for larger tuning currents, the resonator becomes more sensitive to current noise, and most likely owing to mechanical resonances and eddy currents in the coaxial cables excited by the pulse tubes of the cryostat, we saw an increased instability of the resonator frequency at larger magnetic fields. By staying at zero current detuning, we minimize this noise.

In addition, we independently verified the resonator properties using a range of other measurements, including the magnitude of 1/f frequency noise, intrinsic loss tangent, presence of surface paramagnetic spins (via an electron spin resonance spectrum), and the qTLS dependence on a number of external factors. A detailed description and the data of these additional control experiments can be found in the Supplementary Materials, together with the details of the theory developed and electrostatic modeling of the device.

SUPPLEMENTARY MATERIALS

Supplementary material for this article is available at http://advances.sciencemag.org/cgi/content/full/6/51/eabc5055/DC1

REFERENCES AND NOTES

1. P. V. Klimov, J. Kelly, Z. Chen, M. Neeley, A. Megrant, B. Burkett, R. Barends, K. Arya, B. Chiaro, Y. Chen, A. Dunsworth, A. Fowler, B. Foxen, C. Gidney, M. Giustina, R. Graff, T. Huang, E. Jeffrey, E. Lucero, J. Y. Mutus, O. Naaman, C. Neill, C. Quintana, P. Roushan, D. Sank, A. Vainsencher, J. Wenner, T. C. White, S. Boixo, R. Babbush, V. N. Smelyanskiy, H. Neven, J. M. Martinis, Fluctuations of energy-relaxation times in superconducting qubits. *Phys. Rev. Lett.* **121**, 090502 (2018).
2. S. E. de Graaf, A. A. Adamyan, T. Lindström, D. Erts, S. E. Kubatkin, A. Y. Tzalenchuk, A. V. Danilov, Direct identification of dilute surface spins on Al$_2$O$_3$: Origin of flux noise in quantum circuits. *Phys. Rev. Lett.* **118**, 057703 (2017).
3. J. Burnett, L. Faoro, I. Wisby, V. L. Gurtovoi, A. V. Chernykh, G. M. Mikhailov, V. A. Tulin, R. Shaikhaidarov, V. Antonov, P. J. Meeson, T. Lindström, Evidence for interacting two-level systems from the 1/f noise of a superconducting resonator. *Nat. Commun.* **5**, 4119 (2014).
4. A. Bilmes, A. Megrant, P. Klimov, G. Weiss, J. M. Martinis, A. V. Ustinov, J. Lisenfeld, Resolving the positions of defects in superconducting quantum bits. *Sci. Rep.* **10**, 3090 (2020).
5. J. Lisenfeld, A. Bilmes, A. Megrant, R. Barends, J. Kelly, P. Klimov, G. Weiss, J. M. Martinis, A. V. Ustinov, Electric field spectroscopy of material defects in transmon qubits. *npj Quantum Inf.* **5**, 105 (2019).
6. F. Arute, K. Arya, R. Babbush, D. Bacon, J. C. Bardin, R. Barends, R. Biswas, S. Boixo, F. G. S. L. Brandao, D. A. Buell, B. Burkett, Y. Chen, Z. Chen, B. Chiaro, R. Collins, W. Courtney, A. Dunsworth, E. Farhi, B. Foxen, A. Fowler, C. Gidney, M. Giustina, R. Graff, K. Guerin, S. Habegger, M. P. Harrigan, M. J. Hartmann, A. Ho, M. Hoffmann, T. Huang, T. S. Humble, S. V. Isakov, E. Jeffrey, Z. Jiang, D. Kafri, K. Kechedzhi, J. Kelly, P. V. Klimov, S. Knysh, A. Korotkov, F. Kostritsa, D. Landhuis, M. Lindmark, E. Lucero, D. Lyakh, S. Mandrà, J. R. McClean, M. McEwen, A. Megrant, X. Mi, K. Michielsen, M. Mohseni, J. Mutus, O. Naaman, M. Neeley, C. Neill, M. Y. Niu, E. Ostby, A. Petukhov, J. C. Platt,

C. Quintana, E. G. Rieffel, P. Roushan, N. C. Rubin, D. Sank, K. J. Satzinger, V. Smelyanskiy, K. J. Sung, M. D. Trevithick, A. Vainsencher, B. Villalonga, T. White, Z. J. Yao, P. Yeh, A. Zalcman, H. Neven, J. M. Martinis, Quantum supremacy using a programmable superconducting processor. *Nature* **574**, 505–510 (2019).

7. S. Schlör, J. Lisenfeld, C. Müller, A. Schneider, D. P. Pappas, A. V. Ustinov, M. Weides, Correlating decoherence in transmon qubits: Low frequency noise by single fluctuators. *Phys. Rev. Lett.* **123**, 190502 (2019).

8. J. J. Burnett, A. Bengtsson, M. Scigliuzzo, D. Niepce, M. Kudra, P. Delsing, J. Bylander, Decoherence benchmarking of superconducting qubits. *npj Quantum Inf.* **5**, 54 (2019).

9. S. E. de Graaf, L. Faoro, J. Burnett, A. A. Adamyan, A. Y. Tzalenchuk, S. E. Kubatkin, T. Lindström, A. V. Danilov, Suppression of low-frequency charge noise in superconducting resonators by surface spin desorption. *Nat. Commun.* **9**, 1143 (2018).

10. A. Schneider, T. Wolz, M. Pfirrmann, M. Spiecker, H. Rotzinger, A. V. Ustinov, M. Weides, Transmon qubit in a magnetic field: Evolution of coherence and transition frequency. *Phys. Rev. Res.* **1**, 023003 (2019).

11. G. J. Grabovskij, T. Peichl, J. Lisenfeld, G. Weiss, A. V. Ustinov, Strain tuning of individual atomic tunneling systems detected by a superconducting qubit. *Science* **338**, 232–234 (2012).

12. S. Geaney, D. Cox, T. Hönigl-Decrinis, R. Shaikhaidarov, S. E. Kubatkin, T. Lindström, A. V. Danilov, S. E. de Graaf, Near-field scanning microwave microscopy in the single photon regime. *Sci. Rep.* **9**, 12539 (2019).

13. S. E. de Graaf, A. V. Danilov, S. E. Kubatkin, Coherent interaction with two-level fluctuators using near field scanning microwave microscopy. *Sci. Rep.* **5**, 17176 (2015).

14. J. Lisenfeld, G. J. Grabovskij, C. Müller, J. H. Cole, G. Weiss, A. V. Ustinov, Observation of directly interacting coherent two-level systems in an amorphous material. *Nat. Commun.* **6**, 6182 (2015).

15. J. Lisenfeld, A. Bilmes, S. Matityahu, S. Zanker, M. Marthaler, M. Schechter, G. Schön, A. Shnirman, G. Weiss, A. V. Ustinov, Decoherence spectroscopy with individual two-level tunneling defects. *Sci. Rep.* **6**, 23786 (2016).

16. K. Serniak, M. Hays, G. de Lange, S. Diamond, S. Shankar, L. D. Burkhart, L. Frunzio, M. Houzet, M. H. Devoret, Hot nonequilibrium quasiparticles in transmon qubits. *Phys. Rev. Lett.* **121**, 157701 (2018).

17. F. Henriques, F. Valenti, T. Charpentier, M. Lagoin, C. Gouriou, M. Martinez, L. Cardani, M. Vignati, L. Grünhaupt, D. Gisenkova, J. Ferrero, S. T. Skacel, W. Wernsdorfer, A. V. Ustinov, G. Catelani, O. Sander, I. M. Pop, Phonon traps reduce the quasiparticle density in superconducting circuits. *Appl. Phys. Lett.* **115**, 212601 (2019).

18. X. Y. Jin, A. Kamal, A. P. Sears, T. Gudmundsen, D. Hover, J. Miloshi, R. Slattery, F. Yan, J. Yoder, T. P. Orlando, S. Gustavsson, W. D. Oliver, Thermal and residual excited-state population in a 3D transmon qubit. *Phys. Rev. Lett.* **114**, 240501 (2015).

19. P. J. de Visser, J. J. A. Baselmans, S. J. C. Yates, P. Diener, A. Endo, T. M. Klapwijk, Microwave-induced excess quasiparticles in superconducting resonators measured through correlated conductivity fluctuations. *Appl. Phys. Lett.* **100**, 162601 (2012).

20. A. P. Vepsäläinen, A. H. Karamlou, J. L. Orrell, A. S. Dogra, B. Loer, F. Vasconcelos, D. K. Kim, A. J. Melville, B. M. Niedzielski, J. L. Yoder, S. Gustavsson, J. A. Formaggio, B. A. Van Devender, W. D. Oliver, Impact of ionizing radiation on superconducting qubit coherence. *Nature* **584**, 551–556 (2020).

21. L. Cardani, F. Valenti, N. Casali, G. Catelani, T. Charpentier, M. Clemenza, I. Colantoni, A. Cruciani, L. Gironi, L. Grünhaupt, D. Gusenkova, F. Henriques, M. Lagoin, M. Martinez, G. Pettinari, C. Rusconi, O. Sander, A. V. Ustinov, M. Weber, W. Wernsdorfer, M. Vignati, S. Pirro, I. M. Pop, Reducing the impact of radioactivity on quantum circuits in a deep-underground facility. arXiv:2005.02286 (2020).

22. D. C. Moore, S. R. Golwala, B. Bumble, B. Cornell, P. K. Day, H. G. LeDuc, J. Zmuidzinas, Position and energy-resolved particle detection using phonon-mediated microwave kinetic inductance detectors. *Appl. Phys. Lett.* **100**, 232601 (2012).

23. L. J. Swenson, A. Cruciani, A. Benoit, M. Roesch, C. S. Yung, A. Bideaud, A. Monfardini, High-speed phonon imaging using frequency-multiplexed kinetic inductance detectors. *Appl. Phys. Lett.* **96**, 263511 (2010).

24. A. Bespalov, M. Houzet, J. S. Meyer, Y. V. Nazarov, Theoretical model to explain excess of quasiparticles in superconductors. *Phys. Rev. Lett.* **117**, 117002 (2016).

25. C. Carbillet, V. Cherkez, M. A. Skvortsov, M. V. Feigel'man, F. Debontridder, L. B. Ioffe, V. S. Stolyarov, K. Ilin, M. Siegel, C. Noûs, D. Roditchev, T. Cren, C. Brun, Spectroscopic evidence for strong correlations between local superconducting gap and local Altshuler-Aronov density of states suppression in ultrathin NbN films. *Phys. Rev. B* **102**, 024504 (2020).

26. G. Lemarié, A. Kamlapure, D. Bucheli, L. Benfatto, J. Lorenzana, G. Seibold, S. C. Ganguli, P. Raychaudhuri, C. Castellani, Universal scaling of the order-parameter distribution in strongly disordered superconductors. *Phys. Rev. B* **87**, 184509 (2013).

27. W.-T. Liao, T. P. Kohler, K. D. Osborn, R. E. Butera, C. J. Lobb, F. C. Wellstood, M. Dreyer, Scanning tunneling Andreev microscopy of titanium nitride thin films. *Phys. Rev. B* **100**, 214505 (2019).

28. N. A. Saveskul, N. A. Titova, E. M. Baeva, A. V. Semenov, A. V. Lubenchenko, S. Saha, H. Reddy, S. I. Bogdanov, E. E. Marinero, V. M. Shalaev, A. Boltasseva, V. S. Khrapai,

29. A. I. Kardakova, G. N. Goltsman, Superconductivity behavior in epitaxial TiN films points to surface magnetic disorder. *Phys. Rev. Appl.* **12**, 054001 (2019).

29. S. M. Anton, J. S. Birenbaum, S. R. O'Kelley, V. Bolkhovsky, D. A. Braje, G. Fitch, M. Neeley, G. C. Hilton, H.-M. Cho, K. D. Irwin, F. C. Wellstood, W. D. Oliver, A. Shnirman, J. Clarke, Magnetic flux noise in DC SQUIDs: Temperature and geometry dependence. *Phys. Rev. Lett.* **110**, 147002 (2013).

30. E. Paladino, Y. M. Galperin, G. Falci, B. L. Altshuler, 1/f noise: Implications for solid-state quantum information. *Rev. Mod. Phys.* **86**, 361–418 (2014).

31. C. M. Quintana, Y. Chen, D. Sank, A. G. Petukhov, T. C. White, D. Kafri, B. Chiaro, A. Megrant, R. Barends, B. Campbell, Z. Chen, A. Dunsworth, A. G. Fowler, R. Graff, E. Jeffrey, J. Kelly, E. Lucero, J. Y. Mutus, M. Neeley, C. Neill, P. J. J. O'Malley, P. Roushan, A. Shabani, V. N. Smelyanskiy, A. Vainsencher, J. Wenner, H. Neven, J. M. Martinis, Observation of classical-quantum crossover of 1/f flux noise and its paramagnetic temperature dependence. *Phys. Rev. Lett.* **118**, 057702 (2017).

32. C. Müller, J. H. Cole, J. Lisenfeld, Towards understanding two-level-systems in amorphous solids: Insights from quantum circuits. *Rep. Prog. Phys.* **82**, 124501 (2019).

33. P. Kumar, S. Sendelbach, M. A. Beck, J. W. Freeland, Z. Wang, H. Wang, C. C. Yu, R. Q. Wu, D. P. Pappas, R. McDermott, Origin and suppression of 1/f magnetic flux noise. *Phys. Rev. Appl.* **6**, 041001 (2016).

34. B. L. Altshuler, A. G. Aronov, *Electron-electron Interactions in Disordered Systems*, A. L. Efros, M. Pollak, Eds. (North Holland, 1985).

35. Y. Ivry, C.-S. Kim, A. E. Dane, D. De Fazio, A. N. McCaughan, K. A. Sunter, Q. Zhao, K. K. Berggren, Universal scaling of the critical temperature for thin films near the superconducting-to-insulating transition. *Phys. Rev. B* **90**, 214515 (2014).

36. P. N. Chubov, V. V. Eremenko, Y. A. Pilipenko, Dependence of the critical temperature and energy gap on the thickness of superconducting aluminum films. *Sov. Phys. JETP* **28**, 389 (1969).

37. F. Yang, T. Gozlinski, T. Storbeck, L. Grünhaupt, I. M. Pop, W. Wulfhekel, Microscopic charging and in-gap states in superconducting granular aluminum. *Phys. Rev. B* **102**, 104502 (2020).

38. C. H. Wong, F. L. Y. Lam, J. Shen, M. He, X. Hu, R. Lortz, The role of the coherence length for the establishment of global phase coherence in arrays of ultra-thin superconducting nanowires. *Supercond. Sci. Technol.* **30**, 105004 (2017).

39. S. Mahashabde, E. Otto, D. Montemurro, S. E. de Graaf, S. E. Kubatkin, A. V. Danilov, Fast tunable high Q-factor superconducting microwave resonators. *Phys. Rev. Appl.* **14**, 044040 (2020).

40. W. A. Phillips, Two-level states in glasses. *Rep. Prog. Phys.* **50**, 1657–1708 (1987).

41. A. I. Larkin, Y. N. Ovchinnikov, Density of states in inhomogeneous superconductors. *Sov. Phys. JETP* **34**, 1144 (1972).

42. A. Lamacraft, B. D. Simons, Tail states in a superconductor with magnetic impurities. *Phys. Rev. Lett.* **85**, 4783 (2000).

43. A. Silva, L. B. Ioffe, Subgap states in dirty superconductors and their effect on dephasing in Josephson qubits. *Phys. Rev. B* **71**, 104502 (2005).

44. B. I. Halperin, M. Lax, Impurity-band tails in the high-density limit. I. Minimum counting methods. *Phys. Rev.* **148**, 722 (1966).

45. J. Cardy, Electron localisation in disordered systems and classical solutions in Ginzburg-Landau field-theory. *J. Phys. C* **11**, L321–L327 (1978).

46. N. C. Brown, M. Newman, K. R. Brown, Handling leakage with subsystem codes. *New J. Phys.* **21**, 073055 (2019).

47. M. Chand, G. Saraswat, A. Kamlapure, M. Mondal, S. Kumar, J. Jesudasan, V. Bagwe, L. Benfatto, V. Tripathi, P. Raychaudhuri, Phase diagram of the strongly disordered s-wave superconductor NbN close to the metal-insulator transition. *Phys. Rev. B* **85**, 014508 (2012).

48. L. Faoro, L. B. Ioffe, Interacting tunneling model for two-level systems in amorphous materials and its predictions for their dephasing and noise in superconducting microresonators. *Phys. Rev. B* **91**, 014201 (2015).

49. A. Churkin, S. Matityahu, A. O. Maksymov, A. L. Burin, M. Schechter, Anomalous low-energy properties in amorphous solids and the interplay of electric and elastic interactions of tunneling two-level systems. arXiv:2002.02877 (2020).

50. S. E. de Graaf, A. Y. Tzalenchuk, T. Lindström, 1/f frequency noise of superconducting resonators in large magnetic fields. *Appl. Phys. Lett.* **113**, 142601 (2018).

51. F. Yan, S. Gustavsson, A. Kamal, J. Birenbaum, A. P. Sears, D. Hover, T. J. Gudmundsen, D. Rosenberg, G. Samach, S. Weber, J. L. Yoder, T. P. Orlando, J. Clarke, A. J. Kerman, W. D. Oliver, The flux qubit revisited to enhance coherence and reproducibility. *Nat. Commun.* **7**, 12964 (2016).

52. L. B. Nguyen, Y.-H. Lin, A. Somoroff, R. Mencia, N. Grabon, V. E. Manucharyan, High-coherence fluxonium qubit. *Phys. Rev. X* **9**, 041041 (2019).

53. C. Quintana, J. M. Martinis, *Superconducting Flux Qubits for High-connectivity Quantum Annealing without Lossy Dielectrics* (University of California Santa Barbara, 2017).

54. C. Wang, Y. Y. Gao, I. M. Pop, U. Vool, C. Axline, T. Brecht, R. W. Heeres, L. Frunzio, M. H. Devoret, G. Catelani, L. I. Glazman, R. J. Schoelkopf, Measurement and control of quasiparticle dynamics in a superconducting qubit. *Nat. Commun.* **5**, 5836 (2014).

55. K. Karatsu, A. Endo, J. Bueno, P. J. de Visser, R. Barends, D. J. Thoen, V. Murugesan, N. Tomita, J. J. A. Baselmans, Mitigation of cosmic ray effect on microwave kinetic inductance detector arrays. *Appl. Phys. Lett.* **114**, 032601 (2019).

56. S. Fritz, L. Radtke, R. Schneider, M. Weides, D. Gerthsen, Optimization of Al/AlO$_x$/Al-layer systems for Josephson junctions from a microstructure point of view. *J. Appl. Phys.* **125**, 165301 (2019).

57. M. Sidorova, A. Semenov, H.-W. Hübers, K. Ilin, M. Siegel, I. Charaev, M. Moshkova, N. Kaurova, G. N. Goltsman, X. Zhang, A. Schilling, Electron energy relaxation in disordered superconducting NbN films. *Phys. Rev. B* **102**, 054501 (2020).

58. Y. V. Fominov, M. Houzet, L. I. Glazman, Surface impedance of superconductors with weak magnetic impurities. *Phys. Rev. B* **84**, 224517 (2011).

59. T. Proslier, J. F. Zasadzinski, L. Cooley, C. Antoine, J. Moore, J. Norem, M. Pellin, K. E. Gray, Tunneling study of cavity grade Nb: Possible magnetic scattering at the surface. *Appl. Phys. Lett.* **92**, 212505 (2008).

60. H. Huang, C. Padurariu, J. Senkpiel, R. Drost, A. L. Yeyati, J. C. Cuevas, B. Kubala, J. Ankerhold, K. Kern, C. R. Ast, Tunneling dynamics between superconducting bound states at the atomic limit. *Nat. Phys.* 10.1038/s41567-020-0971-0 , (2020).

61. B. W. Heinrich, J. I. Pascual, K. J. Franke, Single magnetic adsorbates on *s*-wave superconductors. *Prog. Surf. Sci.* **93**, 1–19 (2018).

62. T. Lindström, J. Burnett, M. Oxborrow, A. Y. Tzalenchuk, Pound-locking for characterization of superconducting microresonators. *Rev. Sci. Instrum.* **82**, 104706 (2011).

63. J. Burnett, L. Faoro, T. Lindström, Analysis of high quality superconducting resonators: Consequences for TLS properties in amorphous oxides. *Supercond. Sci. Technol.* **29**, 044008 (2016).

Citation: S. E. de Graaf, L. Faoro, L. B. Ioffe, S. Mahashabde, J. J. Burnett, T. Lindström, S. E. Kubatkin, A. V. Danilov, A. Y. Tzalenchuk, Two-level systems in superconducting quantum devices due to trapped quasiparticles. *Sci. Adv.* **6**, eabc5055 (2020).

*Science*Advances

Two-level systems in superconducting quantum devices due to trapped quasiparticles

S. E. de Graaf, L. Faoro, L. B. Ioffe, S. Mahashabde, J. J. Burnett, T. Lindström, S. E. Kubatkin, A. V. Danilov and A. Ya. Tzalenchuk

Use of this article is subject to the Terms of Service